Advanced Pharmaceutical Bulletin

Accepted Manuscript (unedited)

The manuscript will undergo copyediting, typesetting, and review of the resulting proof before it is published in its final form.

Research Article

How to cite this article:
Toroghi F, Jafari-Gharabaghlou D, Najafi R, Mahdavinezhad A, Afshar S, Zarghami N, Amini R. Niosomal Co-delivery of Curcumin and Silibinin Enhances Synergistic Anticancer Activity Against Colorectal Cancer Cells. Advanced Pharmaceutical Bulletin, doi: 10.34172/apb.47534

Niosomal Co-delivery of Curcumin and Silibinin Enhances Synergistic Anticancer Activity Against Colorectal Cancer Cells

Fatemeh Toroghi[1], Davoud Jafari-Gharabaghlou[2], Rezvan Najafi[1], Ali Mahdavinezhad[1], Saeid Afshar[1], Nosratollah Zarghami[2,3], Raziyeh Amini[1]

1. Research Center of Molecular Medicine, Faculty of Medicine, Hamedan University of Medical Sciences, Hamedan, Iran
2. Department of Clinical Biochemistry and Laboratory Medicine, Faculty of Medicine, Tabriz University of Medical Sciences, Tabriz, Iran
3. Department of Medical Biochemistry, Faculty of Medicine, Istanbul Aydin University, Istanbul, Türkiye

ARTICLE INFO

Keywords:
Colorectal Neoplasms;
Nanoparticle;
Drug Delivery System;
Hyaluronic Acid;
Curcumin;
Silibinin

Article History:
Submitted: June 10, 2026
Revised: August 11, 2026
Accepted: August 14, 2026
ePublished: September 05, 2026

ABSTRACT

purpose: Colorectal cancer (CRC) continues to be a major contributor to cancer-related mortality despite advances in diagnosis and management, highlighting the need for targeted, cost-effective therapies. Phytochemicals like curcumin (Cur) and silibinin (Sil) show promising anticancer effects, supported by preclinical and clinical evidence. Nanocarriers, such as niosomes (Nio), enhance the delivery and bioavailability of these bioactive molecules. The present study evaluates the anticancer potency of Cur and Sil, alone and in combination, in free and niosome-encapsulated forms against HCT116 cells, advancing plant-based nanotherapeutics for CRC.

Methods: Niosomes were prepared by thin-film hydration; physicochemical characterization was carried out using DLS, FE-SEM, and FTIR. Cytotoxicity of free, encapsulated, and combined drugs on HCT116 cells was measured using the MTT assay. Cell cycle and apoptosis were analyzed via flow cytometry. Gene expressions of hTERT, BAX, BCL-2, Casp3, Casp7, CCND1, and MMP9 were assessed by qRT-PCR. Cell migration was evaluated with a scratch assay.

Results: The synthesized niosomes exhibited suitable physicochemical characteristics for effective drug delivery. MTT assays demonstrated that both curcumin (Cur) and silibinin (Sil) inhibited r combination – whether free, niosome-encapsulated, or niosome-encapsulated with hyaluronic acid – produced a significant decrease in IC_{50} values. The nano-formulated combination also showed superior induction of apoptosis and cell cycle arrest compared to free drugs. These effects were supported by significant changes in gene expression ($p < 0.05$).

Conclusion: These findings show that co-loaded formulation reduced viability in the tested colorectal cancer cell line, with greater in vitro activity observed for the hyaluronic acid decorated formulation.

***Corresponding Authors**
Nosratollah Zarghmi, Email: zarghamin@gmail.com, ORCID: 0000-0002-4236-4537
Raziyah Amini, Email: aminra14@gmail.com

Introduction

Colorectal cancer (CRC) is the third most diagnosed neoplasm and the second leading cause of neoplasm-related mortality. While CRC incidence rates exhibit geographical variability, a rising global trend has been documented, particularly among individuals younger than 55 years.[1] It is estimated that by 2040, the worldwide incidence of CRC will exceed 3 million new cases, resulting in 1.6 million deaths, predominantly in countries with higher Human Development Index (HDI) scores.[2]

According to U.S. statistical reports, at diagnosis, 38% of CRC patients present with localized tumors, 35% with regional disease, 21% with distant metastases, and 6% remain un-staged.[3] Different therapeutic modalities are available to control CRC; however, the treatment of advanced CRC generally necessitates a multidisciplinary approach that integrates surgery, radiotherapy, and systemic chemotherapy.[4]

Advances in molecular techniques have improved personalized therapy in CRC by enabling treatment selection based on tumor molecular subtypes and aiding prognostic evaluation. Standard systemic treatments for CRC include FOLFOX and FOLFIRI chemotherapy regimens, alongside targeted agents such as EGFR inhibitors for tumors with wild-type RAS and anti-VEGF therapies. Despite progress in these techniques, complete remission is rare, with a median overall survival of around 2-3 years.[5] Patients with CRC often experience serious side effects of current treatments – such as neuropathy, gastrointestinal toxicity, and fatigue – which can limit treatment adherence and reduce quality of life, emphasizing the need for effective and better-tolerated strategies.[6]

Although the use of herbal compounds in traditional medicine spans centuries, recent advances in in vitro experimentation, bioinformatics, and clinical research have increasingly highlighted their therapeutic potential. Numerous phytochemicals, including curcumin, zerumbone, gallic acid, silibinin, berberine, catechin, ursolic acid, quercetin, betulinic acid, and resveratrol, have been identified as bioactive agents with demonstrated anticancer properties.[7-10]

Curcumin, a lipophilic polyphenolic compound, was derived from turmeric by Vogel and Pelletier in 1815. Since then, it has been recognized for its broad-spectrum protective effects against various diseases, including cancer. In cancer cells, curcumin modulates multiple dysregulated signaling pathways involved in proliferation and metabolism, angiogenesis, migration, immune response, and survival. Previous investigations have emphasized that curcumin downregulates oncogenic drivers, including human telomerase reverse transcriptase *(hTERT), Cyclin D1, CDK2, MMP2, MMP9, VEGF, NF-κB*, and *mTOR*. Simultaneously, it upregulates tumor-suppressive molecules, including specific microRNAs, *p21, p27, p53, PTEN, BAX, and BCL2.* [11,12] Moreover, silibinin is a flavonolignan constituent obtained from Silybum marianum seeds. It has demonstrated anti-tumor activity against various cancers, including breast, hepatocellular carcinoma, prostate, and CRC. Although the mechanisms underlying its effects on cancer cells are not yet fully elucidated, substantial evidence supports silibinin's ability to inhibit tumor proliferation, angiogenesis, therapy resistance, and metastasis, as well as to promote programmed cell death.[13-15]

Numerous experimental studies have demonstrated that combining herbal bioactive compounds can produce synergistic or additive effects. Such combinations may enhance bioavailability, reduce the required dosage of individual compounds, thereby minimizing side effects, and simultaneously target multiple molecular pathways.[9,16,17] For instance, co-administration of silibinin and curcumin in DLD-1 and LoVo cell lines has confirmed cell proliferation arrest and increased apoptosis.[18] The results of another experiment revealed that

silibinin, curcumin, and their combination had a time- and dose-dependent cytotoxic effect on breast MCF-7 cells, individually and in combination.[19]

Despite strong evidence of phytochemicals' anticancer efficacy, their clinical application is constrained by insufficient solubility, limited stability, and inadequate bioavailability, thereby reducing their efficacy. To overcome these issues, various nanoscale delivery systems have been developed.[20,21] Among these systems, niosomes are uni- or multilamellar vesicles formed from non-ionic surfactants, offering distinct advantages such as controlled drug release and the ability to encapsulate hydrophilic, lipophilic, and amphiphilic compounds. Additionally, niosomes enhance drug stability and patient compliance while exhibiting osmotic activity, stability, safety, non-immunogenicity, cost-effectiveness, and reduced toxicity, making them a particularly promising platform in nanomedicine.[22,23]

Advances in targeted drug delivery have focused on the development of conjugates that selectively bind to overexpressed receptors on tumor cells, thereby improving therapeutic specificity and minimizing off-target toxicity. Hyaluronic acid (HA) is frequently employed as a targeting ligand due to its biocompatibility, modifiable functional groups (e.g., carboxyl and hydroxyl), and high affinity for CD44 receptors, which are overexpressed in various cancer types.[24] HA-drug conjugates have demonstrated reduced cytotoxicity toward healthy cells and CD44-low cancer cells. These compounds exhibit enhanced efficacy against CD44-overexpressing cells, such as HCT116, compared to the free drug.[25] The current study aimed to analyze the anticancer activity of curcumin and silibinin in HCT116 cells using hyaluronic acid-functionalized niosomal nanoparticles.

Material and methods

Cell lines and chemicals

The HCT116 cells were obtained from the Institute Pasteur Cell Bank in Iran and cultured according to established protocols. Curcumin, silibinin, dimethyl sulfoxide (DMSO), 3-(4,5-dimethylthiazol-2-yl)-2,5-diphenyltetrazolium bromide (MTT), polyethylene glycol (PEG; molecular weight 4,000), polyvinyl alcohol, cholesterol, Span-60, methanol, and chloroform were procured from Sigma Aldrich (St. Louis, MO, USA). Fetal bovine serum (FBS), penicillin-streptomycin antibiotic mixture, and RPMI-1640 culture medium were supplied by Gibco BRL (Gaithersburg, MD, USA). First-strand complementary DNA (cDNA) synthesis kits and SYBR Green PCR Master Mix were provided by Fermentas (Vilnius, Lithuania) and Roche (Mannheim, Germany), respectively.

Preparation of PEGylated noisome

Niosomal nanoparticles were synthesized using the thin-layer hydration method. To prepare 10 mL of drug-free niosomes, 3 mg polyethylene glycol (PEG), 6 mg cholesterol, and 36 mg Span 60 were dissolved in a methanol-chloroform mixture at a weight ratio of 1:2:12, respectively. The organic solvents were evaporated using a rotary evaporator at 55-65℃ for 1 h, starting with 5 min at 0.19 atm, followed by 45 min at 0.46 atm, with stirring at 120 rpm, forming a thin lipid film on the inner surface of the flask.

After cooling to room temperature, 10 mL phosphate-buffered saline (PBS) was added to hydrate the film. The flask was reattached to the rotary evaporator and incubated for 1 h at 55-65℃, 0.09 atm, and 90 rpm stirring. The resulting niosomal suspension was collected and cooled in an ice bath. To reduce size and improve homogeneity, the suspension was sonicated using a probe sonicator at 25% amplitude (200 W) for 30 min at 24℃ (Fisher

Scientific Co., USA). The final niosomal formulation was stored at 4℃. For further stabilization, the samples were freeze-dried using a freeze-drying system (Dena Vacuum, model FD-5005-BT, Iran).

Preparation of hyaluronic acid decorated niosomes

HA-decorated niosomes were prepared by surface functionalization of preformed niosomal nanoparticles. Initially, drug-loaded or drug-free niosomes were synthesized via the thin-film hydration approach as previously described. Subsequently, HA conjugation was achieved by incubating the niosomal suspension with hyaluronic acid under gentle stirring to allow adsorption onto the niosomal surface. Briefly, a solution of 1% (w/v) hyaluronic acid in 10 mL of normal saline was added dropwise to the suspension at ambient temperature. The mixture was stirred for 1 h to facilitate electrostatic interaction and/or covalent binding between HA and the niosome surface. Excess unbound HA was removed by centrifugation at 500 rpm for 15 min, followed by PBS washing. The HA-decorated niosomes were then collected and resuspended in PBS. The final formulation was maintained at 4℃.

Preparation of drug-loaded niosomes

A 10-mL solution of nanocurcumin (1000 μM) was prepared according to the previously established protocol. For drug encapsulation into niosomes, 3.6 mg of curcumin was initially incorporated into the solvent system alongside the other formulation components. The initial concentration of both free curcumin and drug-loaded niosomes was maintained at 1,000 μM. Subsequent dilutions were conducted using RPMI-1640 medium to achieve the desired concentrations. Similarly, silibinin-loaded niosomes were prepared by adding 4.8 mg of silibinin to the solvent mixture together with the remaining formulation constituents during the initial preparation step.

Niosome characterization

particle size, dispersion index, and zeta potential

A dynamic light scattering (DLS) test was carried out using a Zetasizer Nano ZS (Malvern Instruments Ltd., Malvern, UK) to characterize the diameter, zeta potential, and polydispersity index (PDI) of niosomes. Materials were diluted tenfold (1:10) with deionized water to minimize multiple scattering effects and ensure optimal particle concentration for accurate measurements. The PDI value was used to assess the homogeneity and breadth of the nanoparticle population’s size distribution.

Morphology

The morphology and microstructure of the niosomes were characterized using scanning electron microscopy (SEM; MIRA3 TESCAN) and atomic force microscopy (AFM; JPK Instruments AG, Berlin, Germany). SEM provided high-resolution images revealing the overall shape, size, and surface texture of the niosomes, confirming their spherical morphology and uniform size distribution. AFM provided nanoscale surface topography, enabling detailed analysis of surface roughness and structural features of individual vesicles. Together, these complementary techniques validated the successful formation of well-defined, homogenous niosomal vesicles with smooth surfaces, essential for enhanced stability and controlled drug delivery.

Physico-chemistry properties

Fourier-transform infrared (FTIR) spectroscopy was performed using a Shimadzu 8400S spectrometer (Kyoto, Japan) to elucidate molecular structural characteristics and investigate potential chemical interactions between

free drugs and their nanoformulated counterparts. Before the analysis, all samples were lyophilized to achieve complete dehydration and converted to dry powders to eliminate moisture interference. The dry powders were then thoroughly homogenized with spectroscopic-grade potassium bromide (KBr) at an optimized weight ratio (typically 1:100 drug-to-KBr) to ensure adequate sample dispersion and pellet transparency. The mixtures were compressed into uniform, thin pellets under high pressure using a hydraulic press to minimize scattering effects and optimize spectral resolution.

FTIR spectra were collected in the mid-infrared region, from 400 to 4000 cm^{-1}, at a spectral resolution of 4 cm^{-1}, with multiple scans averaged to enhance the signal-to-noise ratio. This spectral range encompasses fundamental vibrational modes, including stretching and bending vibrations of key functional groups such as hydroxyl (O–H), carbonyl (C=O), aromatic C=C, and ether (C–O–C) moieties. Comparative spectral analysis between free and encapsulated drugs was conducted to detect shifts in peak positions, changes in band intensities, or the emergence/disappearance of bands, which may indicate intermolecular interactions such as hydrogen bonding, complexation, or covalent modifications induced by the nano formulation process.

Assessment of encapsulation efficiency (EE)

Calibration curves for curcumin and silibinin were constructed using a series of standard solutions prepared in methanol at known concentrations. To separate free (unencapsulated) drug from encapsulated drug, the niosomal suspension was subjected to centrifugal ultrafiltration using an Amicon MPS device (Millipore, Burlington, MA, USA) and centrifuged using a Hettich benchtop centrifuge (Tuttlingen, Germany). The encapsulated drug remained above the membrane, while the filtrate containing free drug was collected from the lower compartment and subsequently analyzed.

Entrapment efficiency (EE%) was determined using the following formula:

$$\text{EE}\ (\%) = \left(\frac{\text{Total drug} - \text{Free drug}}{\text{Total drug}}\right) \times 100$$

This index validated that the UV spectrophotometric method ensured accurate and reproducible quantification of unencapsulated curcumin and silibinin, enabling reliable examination of drug loading and encapsulation efficiency in the niosomal formulations.

In Vitro Drug Release Study

The release of curcumin and silibinin from niosomes was measured using a dialysis diffusion method. A known quantity of drug-loaded niosomes (equivalent to 25 mg of formulation) was suspended in PBS (pH 7.4) and transferred into a dialysis bag with a molecular weight cut-off (MWCO) of 12 kilodaltons. The sealed dialysis bags were immersed in 50 mL of PBS and incubated at 37 ± 0.5℃ with continuous stirring at 120 rpm to simulate a biological environment.

At defined time points, 2 mL aliquots of the release medium were withdrawn and replaced with the same volume of fresh, pre-warmed PBS to maintain sink conditions. The concentrations of curcumin and silibinin in the external medium were quantified by UV-Vis spectrophotometry (PerkinElmer, Fremont, CA, USA) at their respective absorbance maxima: 425 nm for curcumin and 287 nm for silibinin. The cumulative percentage of drug secretion

was assessed and plotted over time to determine the release kinetics and efficiency of the niosomal delivery system.

Cell culture

HCT116 cells were grown in RPMI-1640 medium supplemented with 10% fetal bovine serum (FBS), 0.05 mg/mL penicillin G, and 0.08 mg/mL streptomycin at 37℃ in a humidified incubator with 5% CO_2 atmosphere.

Cytotoxic test

Since its introduction, the MTT assay has been widely accepted and reliable for assessing the cytotoxicity of therapeutic agents on cancer cell proliferation and for investigating potential synergistic effects between compounds such as curcumin and silibinin, both in free and niosome-encapsulated forms, as well as their combinations. The cytotoxicity of free drugs, niosome-loaded drugs, and their combinations was estimated using the MTT assay. HCT116 cells were cultured at a density of 2×10^4 cells per well in 96-well plates and incubated for 24 h at 37℃ with 5% CO_2 to provide for cell adherence. Subsequently, cells were exposed to varying concentrations of free and nano-formulated curcumin, silibinin, and their combination for 48 h. Blank niosomes served as vehicle controls, and untreated cells were included as negative controls.

Following treatment, the culture medium was replaced with 200 µL of phosphate-buffered saline (PBS) containing 0.5 mg/mL MTT reagent (Sigma, Germany). Plates were covered with aluminum foil to protect from light and incubated for 4 h at 37℃ to facilitate formazan crystal formation. Then, the MTT solution was removed, and 100 µL of dimethyl sulfoxide (DMSO) and 25 µL of Sorensen's glycine buffer were added to each well to dissolve the formazan crystals. The plates were shaken gently for 15 min.

Absorbance was quantified at 570 nm, with a reference wavelength of 630 nm, using the BioTek PowerWave XS ELISA microplate reader. Cell viability was quantified as a percentage relative to untreated controls. The half-maximal inhibitory concentration (IC_{50}) values were determined using nonlinear regression analysis. The experiments were performed in triplicate. Statistical significance between treatment groups was determined using one-way analysis of variance (ANOVA) followed by Tukey's post hoc test; p-values < 0.05 were considered statistically significant.

Real-Time PCR Analysis

Cell Culture and Treatment:

HCT116 cells were cultured at a quantity of 4×10^6 cells per well in six-well plates and incubated at 37℃ in a humidified atmosphere containing 5% CO_2 for 24 h. After cell adherence, treatments were applied using free or nano-formulated curcumin and silibinin, both individually and in combination, at their respective IC_{50} concentrations.

RNA Extraction and Quantification:

Total RNA was collected from treated and control cells using TRIzol reagent (Sigma, Roedermark, Germany) according to the manufacturer's protocol. The quality of harvested RNA was calculated by assessing the absorbance ratio at 260/280 nm ($OD_{260}/_{280}$) using a spectrophotometer.

cDNA Synthesis:

Complementary DNA (cDNA) synthesis was performed using the First-Strand cDNA Synthesis Kit (Fermentas,

Vilnius, Lithuania). Each 20 µL reverse transcription reaction contained 5 µL of total RNA, 1 µL of random hexamer primers, and 14 µL of cDNA master mix. The reactions were incubated at 50℃ for 30 min, followed by enzyme deactivation at 90℃ for 5 min.

Quantitative Real-Time PCR:

The transcriptional intensity of *hTERT, BAX, BCL2, CASP3, CASP7, and CCND1* was quantified using a Bio-Rad IQ5 Real-Time PCR system (Hercules, CA, USA). Amplification was carried out using Hot Taq EvaGreen qPCR and SYBR Master Mix (Life Technologies Applied Biosystems, UK). *GAPDH* served as the endogenous control gene. Primer sequences were designed and verified using Primer-BLAST (NCBI) (Table 1).

Table 1: Primer sequences used for real-time PCR amplification; Expression of seven genes was analyzed using RT-PCR: human telomerase reverse transcriptase (hTERT), B-cell lymphoma 2 protein (Bcl2)-associated X (BAX), B-cell leukemia/lymphoma 2 protein (BCL2), apoptosis-related cysteine peptidase 3 and7 (CASP3 and CASP7), Cyclin D1 (CCND1), Matrix metalloproteinase-9 (MMP9), and Glyceraldehyde 3-phosphate dehydrogenase (GAPDH) as reference gene.

Genes	Forward (5′ → 3′)	Reverse (5′ → 3′)
hTERT	CTTTTATGTCACGGAGACCACGTT	AGTGCTGTCTGATTCCAATGCTT
BAX	ACGTGGGCATTTTTCTTACTTT	TATTACCCCCTCAAGACCACT
BCL2	AAACTTGACAGAGGATCATGC	ATCTTTATTTCATGAGGCACGTT
CASP3	CCTTCCATCAAATAGAACCAC	ATTGCCTCTCATAATGACTGC
CASP7	GCCAAGGGGATATTTACTGCT	CATGAAAATCTGCCCTAAGCC
CCND1	CACTTTCAGTCCAATAGGTGT	AACAAGTACATGGATATTCCC
MMP9	CCACTACTGTGCCTTTGAGTCC	AGAGAATCGCCAGTACTTCCC
GAPDH	AACGACCACTTTGTCAAGCTC	TTGCTGTAGCCAAATTCGTTG

The PCR cycling conditions were as follows: a first melting step at 95℃ for 10 min; 40 cycles of denaturation at 95℃ for 15 seconds, annealing at 60℃ for 30 seconds, and extension at 72℃ for 30 seconds; followed by a melting curve analysis from 65℃ to 95℃ to confirm product specificity.

Data Analysis:

Relative gene expression was assessed using the comparative Ct (ΔΔCt) method, normalizing target gene expression to GAPDH and reporting fold changes relative to untreated controls. All experiments were carried out in triplicate.

Flow Cytometry Analysis for Cell Death Quantification

Flow cytometry was employed to quantitatively assess cell viability, apoptosis, and necrosis in HCT116 colorectal carcinoma cells. Cells were plated at 4×10^4 cells per well in 6-well plates and incubated under standard conditions (37℃, 5% CO_2) for 24 h to attach. Subsequently, cells were incubated with free drugs, nano-formulated drugs, or their combination at IC_{50} concentrations, with each treatment performed in triplicate. After 48 h, cells were harvested by trypsinization using 0.25% trypsin-EDTA (Sigma, Germany), followed by three washes with phosphate-buffered saline (PBS, pH 7.4) to remove residual media and detached cells. Cells were pelleted by centrifugation at 190 × g for 5 min at room temperature and fixed in 70% ethanol to preserve cellular morphology.

Apoptotic and necrotic cells were distinguished using dual staining with Annexin V conjugated to fluorescein isothiocyanate (FITC) and propidium iodide (PI). Afterward, the cells were subjected to the staining reagents for 20 min at ambient temperature in the dark to prevent photobleaching. Before analysis, 100 µL of binding buffer (0.1 M HEPES, pH 7.4; 1.4 M NaCl; 25 mM $CaCl_2$) was added to each sample to facilitate optimal Annexin V binding.

Data acquisition was conducted on a flow cytometer (Thermo Fisher Scientific, USA). Analysis distinguished viable cells (Annexin V^-/PI^-), early apoptotic cells (Annexin V^+/PI^-), and late apoptotic/necrotic cells (Annexin V^+/PI^+), enabling quantification of cell death modes induced by treatments.

Cell cycle analysis

A total of 5×10^5 HCT116 cells were seeded into each well of a six-well plate and incubated overnight at 37℃ in a humidified atmosphere containing 5% CO_2 to permit cell adhesion. Following incubation, cells were exposed to free and nano-formulated curcumin and silibinin, individually and in combination, at concentrations corresponding to their IC_{50} for 48 h. After treatment, cells were harvested and washed in triplicate with PBS to remove residual media and compounds. The cells were then fixed in 70% ethanol and stored at -20℃ for 48 h.

Before analysis, fixed cells were resuspended in PBS and stained with a solution containing 100 µg/mL propidium iodide (PI) and 1 µg/mL RNase A to quantify DNA content. Samples were maintained at 37℃ for 30 min in the dark to ensure complete staining and RNA digestion. DNA content and cell cycle distribution were investigated by flow cytometry using a BD FACSCanto II system (BD Biosciences, USA). Fluorescence intensity data were collected to estimate the proportion of cells in G0/G1, S, and G2/M phases.

Statistical analysis

Statistical analysis was performed using a two-way ANOVA followed by Tukey's post-hoc test using SPSS and GraphPad Prism (version 8). In this research, $p \leq 0.05$ was considered statistically significant. The results were expressed as the mean ± standard deviation (SD) of three independent experiments.

Results and discussion

Characterization and morphology of nanoparticles

DLS analysis showed that the mean diameters of blank niosomes, curcumin-loaded niosomes, silibinin-loaded niosomes, curcumin/silibinin-loaded, and curcumin/silibinin-loaded HA-niosomes were 158±6.32 nm, 174±6.14 nm, 171±7.62 nm, 199.2±11.3 nm, and 209±17.5 nm, respectively (Figure 1).

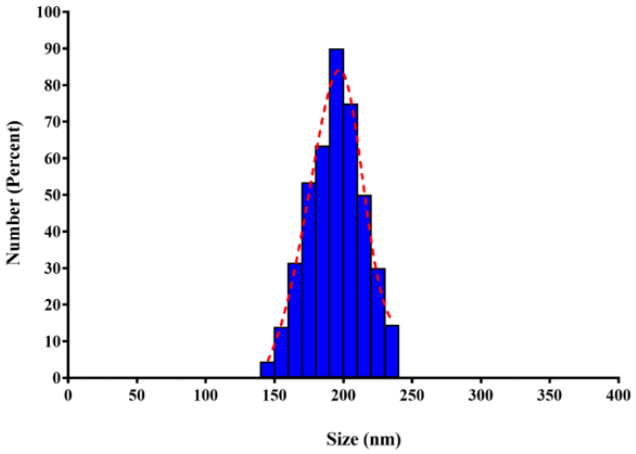

Figure 1. The DLS analysis on the mean diameter of curcumin/silibinin-hyaluronic acid decorated niosomes; Nanoparticles sized 100-250 nm fall within the optimal range for efficient cellular uptake in solid tumors and extended systemic circulation.

The increase in particle size following drug loading confirms successful encapsulation. The larger size of drug-loaded nanoparticles compared with blank niosomes indicates effective drug incorporation. These size ranges fall within the optimal nanometer scale (100-250 nm), which is critical for efficient cellular uptake in solid cancers and prolonged circulation in systemic delivery, via mechanisms such as the enhanced permeability and retention effect.[26,27]

PDI values were 0.512, 0.672, 0.593, 0.638, and 0.731 for blank, curcumin-loaded, silibinin-loaded, curcumin/silibinin-loaded, and curcumin/silibinin-loaded HA-niosomes, respectively. Zeta potential measurements revealed surface charges of -12.3±1.6 mV, -18.7±2.8 mV, -19.6±2.5 mV, -22.8±4.3, and -21.2±3.3 mV for blank, curcumin-loaded, silibinin-loaded, and curcumin/silibinin-loaded, and curcumin/silibinin-loaded HA-niosomes, respectively (Table 2).

SEM images confirmed that both blank and drug-loaded niosomes possessed spherical morphology without aggregation or pores (Figure 2). AFM analysis corroborated the SEM and DLS results, revealing curcumin and silibinin-loaded niosomes (Figure 3). The smaller sizes observed via AFM compared to DLS are attributed to sample dehydration during AFM imaging, which eliminates the hydration shell measured by DLS. Collectively, these physicochemical characterizations validate the successful preparation of stable, uniformly sized niosomal nanoparticles with efficient drug encapsulation and favorable properties for enhanced drug delivery.

Table 2: Characterization of Niosomes using DLS; B-Nio: blank noisome, Cur-Nio: curcumin-loaded niosomes, Sil-Nio: silibinin-loaded niosomes, Cur/Sil-Nio: curcumin and silibinin-loaded niosomes, Cur/Sil-H-Nio: curcumin and silibinin-loaded hyaluronic acid decorated niosomes.

Sample groups	Size (nm)	Polydispersity index	ζ-Potential (mV)
B- Nio (mean ± SD)	158±6.32	0.512	−12.3±1.6
Cur-Nio (mean ± SD)	174±6.14	0.672	−18.7±2.8
Sil-Nio (mean ± SD)	171±7.62	0.593	−19.6±2.5
Cur/Sil-Nio (mean ± SD)	199.2±11.3	0.638	−22.8±4.3
Cur/Sil-H-Nio (mean ± SD)	209±17.5	0.731	−21.2±3.3

SEM images confirmed that both blank and drug-loaded niosomes possessed spherical morphology without aggregation or pores (Figure 2). AFM analysis corroborated the SEM and DLS results, revealing curcumin and silibinin-loaded niosomes (Figure 3). The smaller sizes observed via AFM compared to DLS are attributed to sample dehydration during AFM imaging, which eliminates the hydration shell measured by DLS. Collectively, these physicochemical characterizations validate the successful preparation of stable, uniformly sized niosomal nanoparticles with efficient drug encapsulation and favorable properties for enhanced drug delivery.

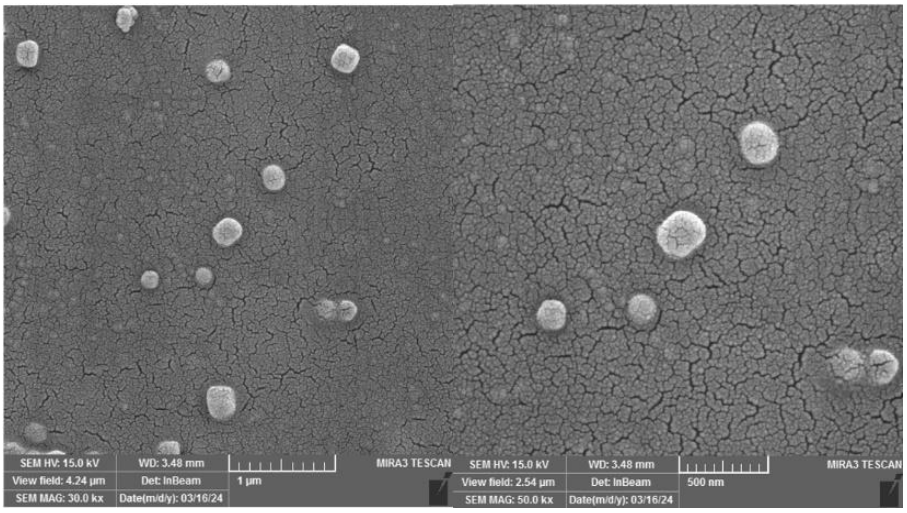

Figure 2. SEM image of drug-loaded niosomal nanoparticles; The micrograph demonstrated spherical morphology of niosomes, with no observable aggregation or porosity.

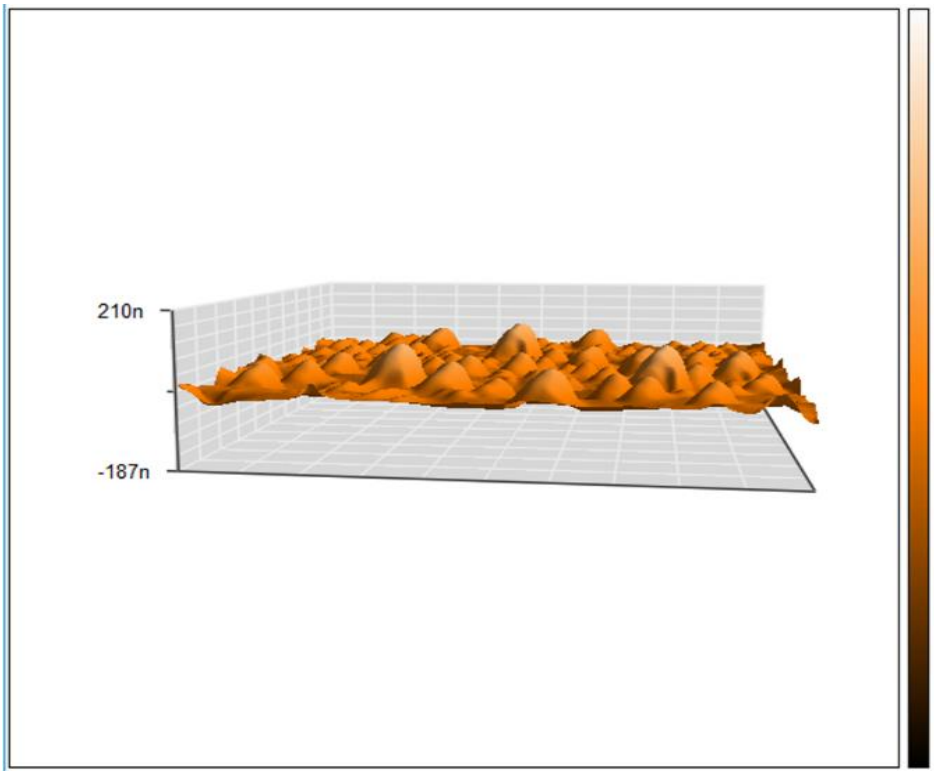

Figure 3. AFM image of drug-loaded niosomal nanoparticles; AFM observations corroborated SEM and DLS data, revealing curcumin- and silibinin-loaded niosomes, with the reduced sizes in AFM attributed to dehydration effects

FTIR spectroscopy was used to assess the physical state of the drugs and evaluate the chemical compatibility between the active pharmaceutical ingredient, hyaluronic acid, and the various components of the niosomal formulation. This analysis provided detailed insight into molecular interactions by identifying characteristic functional group vibrations and spectral changes indicative of possible interactions (Figure 4).

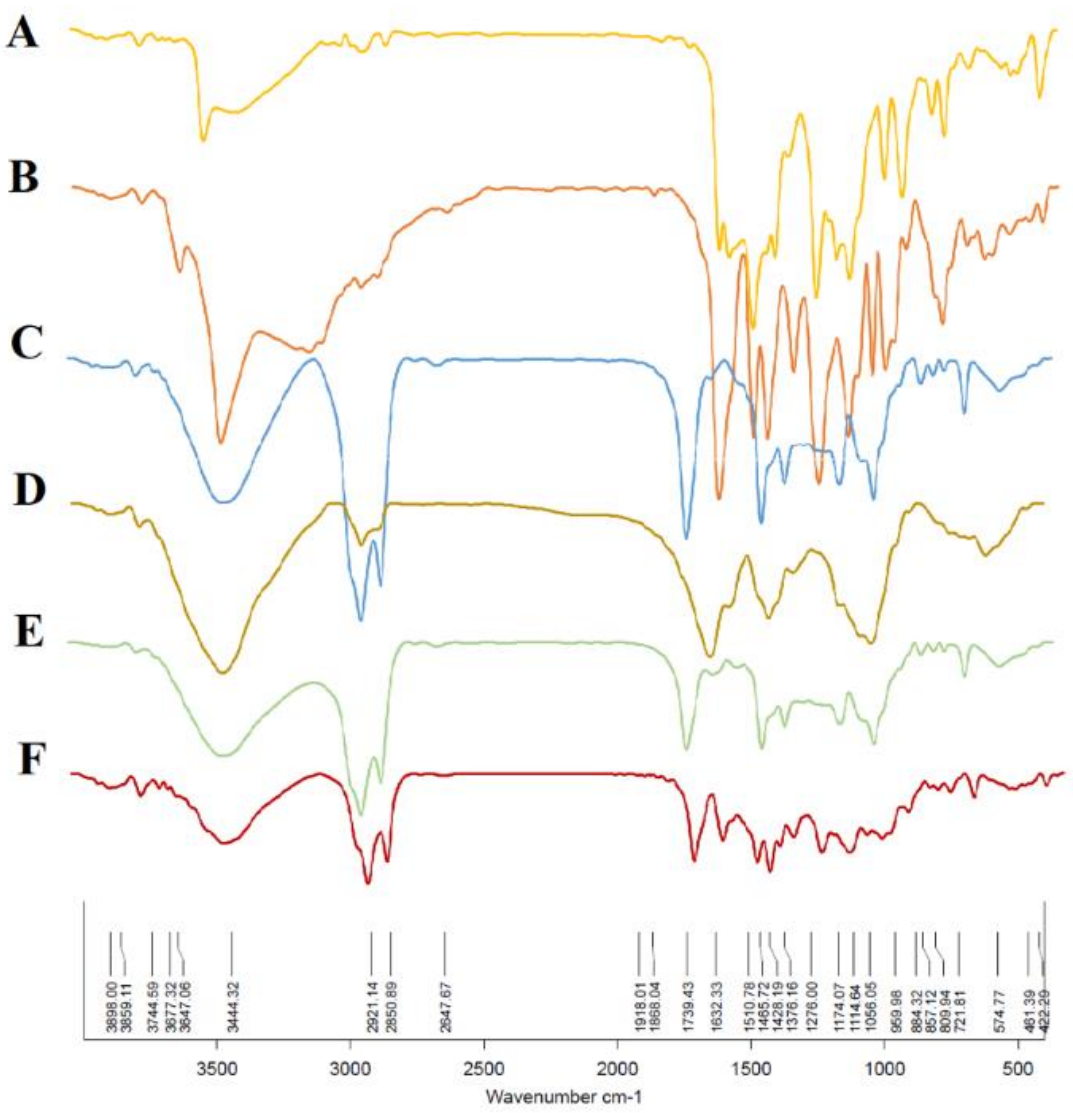

Figure 4. FTIR spectra confirmed key functional groups: curcumin (O–H, C=C, C–O–C, aromatic C–H), silibinin (O–H, C=O, aromatic C=C, phenolic C–O), hyaluronic acid (O–H, amide I/II, C–O–C), and niosomal carriers (C–H, C=O, C–O–C, OH), consistent with their chemical structures. (A: curcumin, B: silibinin, C: niosome, D: hyaluronic acid, E: - hyaluronic acid decorated niosome, F: curcumin/ silibinin hyaluronic acid decorated niosome)

For *curcumin*, key FTIR peaks include a broad O–H stretching band near 3490 cm^{-1}, characteristic of hydroxyl groups involved in hydrogen bonding. Aromatic C=C stretching vibrations are observed around 1620 cm^{-1}, while symmetric C–O–C stretching of methoxy groups appears near 1,248 cm^{-1}. Aromatic C–H bending is evident at approximately 991 cm^{-1}, corresponding to curcumin's hydroxyl, aromatic, and methoxy functional groups.

Silibinin exhibits prominent FTIR peaks including a broad O–H stretch near 3400 cm^{-1}, representing hydroxyl groups; carbonyl (C=O) stretching vibrations between 1650 and 1600 cm^{-1}; aromatic C=C stretching bands between 1600 and 1500 cm^{-1}; and C–O stretching vibrations of phenolic groups between 1300 and 1250 cm^{-1}. These peaks confirm the presence of silibinin's hydroxyl, carbonyl, aromatic, and phenolic groups.

Hyaluronic acid shows characteristic FTIR absorption bands such as a broad O–H stretching band around 3,400 cm^{-1} due to hydroxyl and carboxylic acid groups. The C=O stretching (amide I) appears near 1,630 cm^{-1}, while

N–H bending (amide II) is typically observed around 1,540 cm^{-1}. Additionally, C–O–C stretching vibrations of glycosidic linkages are detected near 1,050 cm^{-1}. These peaks confirm the polysaccharide structure and functional groups of hyaluronic acid.

The *niosomal carrier* mainly consists of non-ionic surfactants (e.g., Span or Tween) and cholesterol. FTIR spectra typically show characteristic alkyl C–H stretching bands near 2,920 and 2,850 cm^{-1}, corresponding to stretching of methylene units. The ester C=O stretching of the surfactant appears near 1,735 cm^{-1}, while C–O–C ether stretching is detected around 1,100-1,150 cm^{-1}. Cholesterol's OH group produces a broad band near 3400 cm^{-1}, overlapping with other hydroxyl-containing components.

The FTIR spectrum of the drug-loaded formulation exhibited all characteristic peaks of curcumin, silibinin, hyaluronic acid, and the niosomal carrier, with no new bands indicating chemical bond formation. Minor shifts or broadening of certain peaks were observed, likely due to hydrogen bonding and hydrophobic interactions among the drugs, hyaluronic acid, and the niosomal bilayer. These interactions reflect physical encapsulation rather than covalent bonding.

The retention of drug-specific and carrier-specific peaks confirms the chemical integrity of both drugs and excipients within the PEGylated niosomes coated with hyaluronic acid. This result suggests successful physical encapsulation without chemical interaction or degradation, which is essential for maintaining drug efficacy and formulation stability.

Drug entrapment efficiency

The drug entrapment efficiency assessment revealed that the entrapment efficiencies of curcumin and silibinin in the niosomes were 76 and 79, respectively, indicating effective encapsulation of both hydrophobic compounds within the niosomal bilayer.

These high entrapment efficiencies suggest that niosomal formulation provides an efficient delivery system, potentially enhancing the bioavailability of nanodrugs and controlled release.

Drug release analysis

A drug release study was done using the dialysis method under both physiological (pH 7.4) and tumor microenvironment-mimicking acidic (pH 4.4) parameters. The release pattern of curcumin and silibinin from the niosomal formulations was evaluated in phosphate-buffered saline (PBS) at 37℃ over 96 h. By the end of the study, approximately 39% and 78% of curcumin and 40.5% and 82% of silibinin were released at pH 7.4 and pH 4.4, respectively (Figure 5). These results demonstrate significantly enhanced drug release under acidic conditions, suggesting improved therapeutic performance of the drug-loaded nanoparticles within the tumor microenvironment.

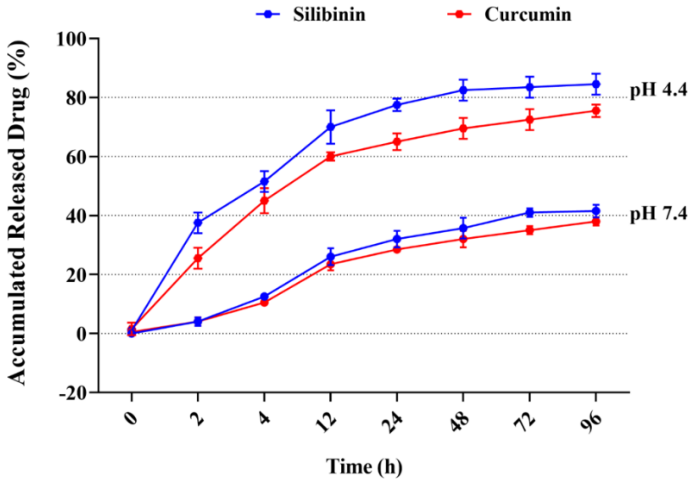

Figure 5. In vitro release pattern of curcumin and silibinin from niosomes in 96 h in two physiological pH (7.4) and acidic pH (4.4); Enhanced release in acidic environments highlights the potential of drug-loaded nanoparticles for effective tumor-targeted therapy.

The biphasic release pattern can be attributed to the bilayer structure of the niosomes. The initial burst phase reflects the release of drug molecules loosely associated with the vesicle exterior, followed by a sustained release stage governed by diffusion through the nanoparticle bilayer. This controlled release pattern supports prolonged therapeutic drug levels, reduced dosing frequency, and lower systemic toxicity. The faster release observed at acidic pH further indicates pH-responsive behavior, enabling preferential drug release within the acidic tumor microenvironment while limiting premature leakage under physiological conditions. Such pH-sensitivity enhances the effective bioavailability of curcumin and silibinin, whose clinical utility is typically constrained by low solubility and stability.[15,28]

In vitro cytotoxicity

The MTT assay was performed after 48 h of drug treatment (Figure 6). Our results demonstrated that both curcumin and silibinin inhibited HCT116 cell growth in a dose- and time-dependent manner, consistent with previous studies.[29,30] The nano-formulated curcumin and silibinin exhibited greater cytotoxicity compared to their free counterparts at equivalent doses. This improved cytotoxic activity may be attributed to the unique physicochemical properties of niosomes, which enhance drug solubility and bioavailability in aqueous environments and facilitate more efficient, targeted intracellular delivery to cancer cells. Similar observations have been reported in multiple prior studies.[31,32]

Notably, treatment with empty niosomes showed no significant cytotoxicity, with over 90% cell viability, confirming the niosomal carrier's high biocompatibility and supporting its suitability as a drug delivery vehicle. For further studies, the following concentrations were selected based on IC_{50} values and cytotoxicity data: 11.3 µM for free curcumin, 8.2 µM for nano-curcumin, 23.4 µM for free silibinin, 19.7 µM for nano silibinin, 3.9 µM and 9.1 µM for free curcumin/silibinin combination, 2.8 µM and 6.5 µM for nano-curcumin/ silibinin combination, and 2.1 µM and 4.6 µM for HA-nano-curcumin/ silibinin combination.

In addition, to distinguish the nature of the interaction between curcumin and silibinin in combination form, combination effect (CI) was calculated for the selected formulation ratio using median-effect method (Table 3).

CI value greater than, equal to, or less than 1 indicates antagonistic, additive, or synergistic influence, respectively. The CI values for free, niosomal, and HA- niosomal combination of curcumin and silibinin were 0.69, 052, and 0.44, respectively. Greater in vitro activity of co-loaded formulation is consistent with earlier documents highlighting the benefits of combination therapy in reducing dosage requirements, and following side effects.[13,33] Comprehensive synergy evaluation requires additional dose-matrix experiments and formal interaction analysis.

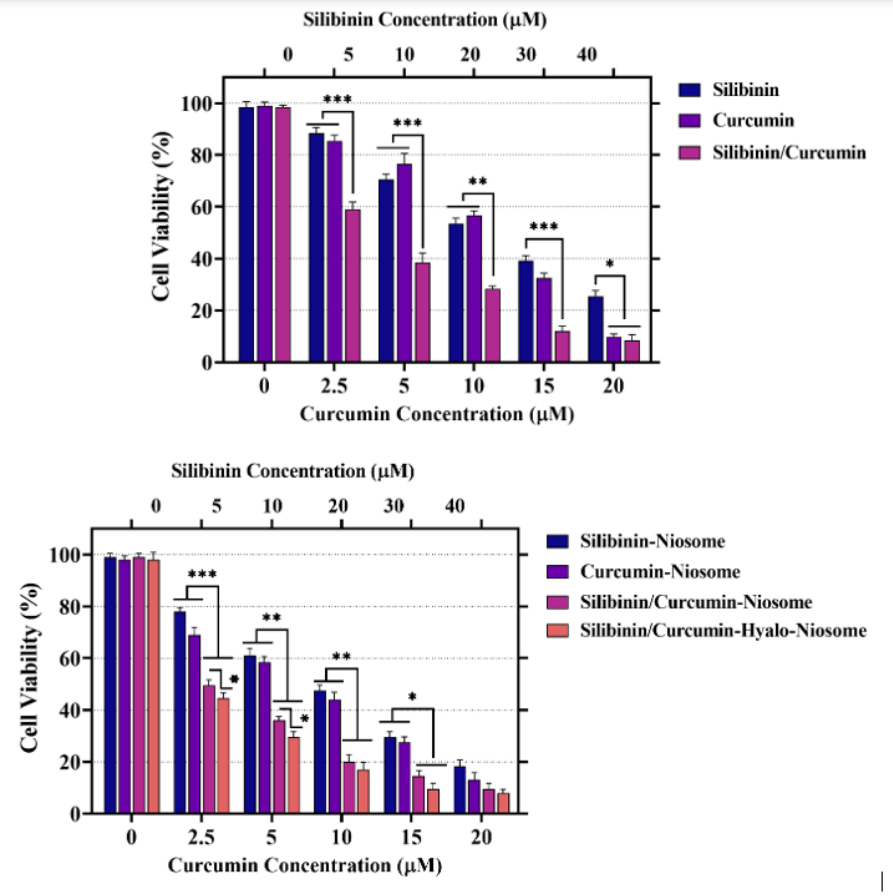

Figure 6. MTT assay results in the HCT116 cell line after treatment with free (left) and nano (right) forms of curcumin and silibinin; Nano-formulated curcumin and silibinin exhibited greater cytotoxicity than free drugs, and their combination synergistically inhibited HCT116 cell proliferation.

Table 3. IC_{50} values and combination indexes

Form	Silibinin	Curcumin	Curcumin in combination	Silibinin in combination	Combination index
Free	23.4 µM	11.3 µM	3.9µM	9.1 µM	0.69
Nano	19.7 µM	8.2 µM	2.8 µM	6.5 µM	0.52
Hyalo-decorated-Nano	-	-	2.1 µM	4.6 µM	0.44

Gene expression assessment

The transcriptional levels of seven genes implicated in cell proliferation, survival, apoptosis, and metastasis were quantified by RT-PCR. Telomere elongation is mediated by telomerase, an RNA-dependent DNA polymerase with two core components: the RNA subunit (hTR) and the catalytic protein subunit (hTERT). The enzyme activity and *hTERT* expression are normally restricted to embryonic and pluripotent stem cells but are reactivated in approximately 85-90% of cancers, contributing to unlimited proliferative capacity and cellular immortality.[34]

Among apoptosis-regulating genes, *BAX* (pro-apoptotic) and *BCL2* (anti-apoptotic) are key members of the BCL2 family that modulate mitochondrial outer membrane permeability. Elevated *BAX* promotes apoptosis, whereas increased *BCL2* expression is linked to radio-resistance in cancer cells.[35] Previous literature has reported that curcumin and silibinin downregulate *hTERT* and *BCL2*, as well as upregulating *BAX* and *CASP3*, thereby promoting apoptotic signaling.[36] Activation of Bax triggers mitochondrial membrane permeabilization, facilitating the liberation of cytochrome c into the cytosol. Cytochrome c subsequently binds Apaf-1, facilitating apoptosome formation and activation of caspase 9. As an initiator caspase, caspase-9 triggers downstream effectors, including caspases 3 and 7.[37] Numerous studies highlight the central role of these proteases in determining cell survival or death. In this respect, caspase-3 expression and activity are considered strong predictors of cancer cell fate and patient prognosis.[38]

Cyclin D1, an important mediator of the G1-to-S phase transition, is frequently upregulated in malignancies. Previous research has demonstrated that its downregulation suppresses cell-cycle progression across various cancer type.[39] Both curcumin and silibinin – whether administered in free form or encapsulated in niosomes – have been shown to reduce *CCND1* expression.[40,41]

Consistent with these findings, our results (Fig. 7) show that curcumin and silibinin, in both free and niosomal formulations, modulate gene expression to suppress cell proliferation, induce apoptosis, and inhibit metastatic potential. As in earlier experiments within this study, a clear greater effect was observed with the combined treatment in certain anti-cancer genes expression levels.

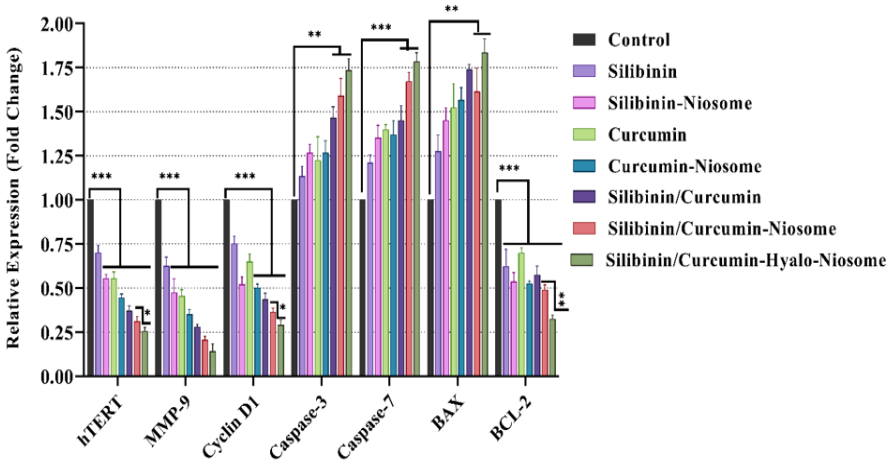

Figure 7. Fig. 7. Differentiation in gene expression; RT-PCR analysis of seven genes involved in proliferation, survival, apoptosis, and metastasis revealed that curcumin and silibinin, in both free and niosomal forms, modulate gene expression to suppress cell proliferation, downregulate hTERT and BCL2, and upregulate BAX, CASP3, and other pro-apoptotic markers. CCND1 expression was also reduced, indicating cell-cycle arrest. Niosomal formulations, particularly in combination, exhibited enhanced pro-apoptotic effects in HCT116 cells, consistent with their potential to inhibit tumor growth and metastatic potential (ns: $P > 0.05$, *: $P \leq 0.05$, **: $P \leq 0.01$, ***:$P \leq 0.001$)

Apoptosis

Cancer is characterized by widespread dysregulation of gene expression and protein activity, creating multiple potential therapeutic targets. Apoptosis is one such critical pathway; an imbalance between pro-apoptotic and anti-apoptotic gene expression suppresses programmed cell death and contributes to drug resistance.[42] Numerous studies have demonstrated that natural compounds such as curcumin and silibinin can promote apoptosis,[19,43,44] supporting their potential as low-risk anticancer agents through apoptosis induction.[45] In the present study, both curcumin and silibinin effectively induced apoptosis in HCT116 cells, with their niosomal formulations (individually and in combination) exhibiting a greater pro-apoptotic effect than the free drugs (Figure 8). These findings align with previous reports.[26,29,46]

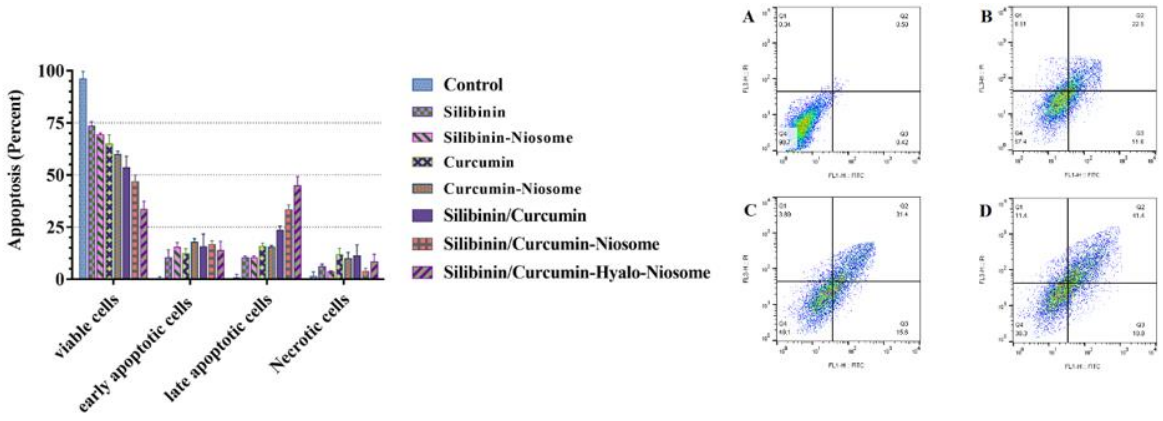

Figure 8. Apoptosis assay: Curcumin and silibinin, in free and niosomal forms, induce apoptosis in HCT116 cells, with niosomal formulations (especially combined treatment), showing the strongest pro-apoptotic effect.

Cell cycle

The cell cycle comprises a coordinated chain of reactions that regulate cellular growth and division. Flow cytometry provides a precise manner for analyzing the cell cycle at the single-cell level.[47] Prior studies have demonstrated that both free and niosomal phytochemicals can induce cell-cycle arrest in various tumor types.[48] In the present experiment, we tested the inhibitory impact of free and niosomal formulations of curcumin and silibinin, individually and in combination, on cell-cycle progression.

Consistent with previous reports,[49,50] treatment with curcumin and silibinin suppressed cell-cycle progression, resulting in arrest in Sub G1 (Figure 9). The control group exhibited a normal distribution of cells across the G0/G1, S, and G2/M phases. In contrast, the treated groups showed the emergence of a sub-G1 population, indicative of apoptotic DNA fragmentation. Our results also revealed that the niosomal formulations exerted a stronger inhibitory influence on the cell cycle than the free drugs. Furthermore, combination therapy, in free or encapsulated form, produced greater suppression than either agent alone.

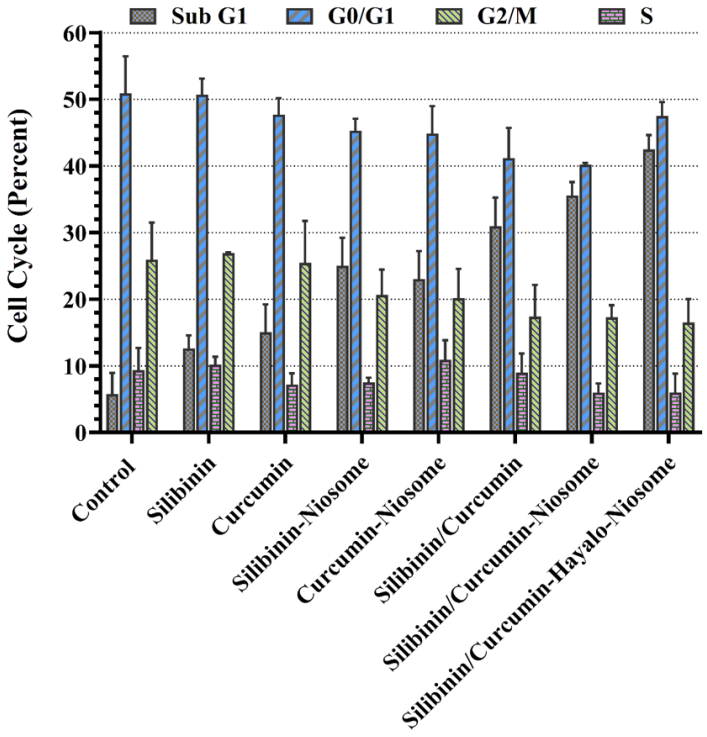

Figure 9. Cell cycle distribution by PI staining represents the percentage of cells in each phase. Flow cytometry analysis of HCT116 cells shows that treatment with free or niosomal curcumin and silibinin, alone or in combination, induces cell-cycle arrest at G1/G1–S transition. Niosomal formulations and combination therapy produced the strongest inhibition, with a sub-G1 population indicative of apoptosis.

Conclusion

This study investigated the anticancer potential of curcumin and silibinin, administered as free compounds and as nano encapsulated formulations, in the HCT116 colorectal cancer cell line. PEGylated niosomal nanocarriers were successfully engineered to enhance the delivery and therapeutic performance of these poorly water-soluble phytochemicals. Across multiple in vitro assays, nano formulations of both curcumin and silibinin demonstrated significantly greater anticancer activity than their corresponding free compounds. Notably, the co-delivery of nano-curcumin and nano-silibinin produced enhanced therapeutic efficacy, which was further augmented by hyaluronic acid surface modification, highlighting the potential of CD44-targeted nanocarrier systems to improve cellular uptake and intracellular drug accumulation.

Despite these promising findings, the present study is limited to a single CRC cell line. Although our results are consistent with previous reports demonstrating the antitumor activity of curcumin and silibinin in diverse cancer models, comprehensive validation in additional colorectal cancer cell lines, normal colonic epithelial cells, and appropriate in vivo models is required to establish therapeutic efficacy, biosafety, pharmacokinetic behavior, and the molecular mechanisms underlying the observed effects.

Furthermore, mechanistic confirmation of CD44 receptor-mediated targeting will require receptor expression profiling, receptor-blocking and competitive inhibition studies, as well as quantitative cellular uptake analyses. Additional investigations employing pharmacological inhibitors, rescue experiments, or gene-silencing

approaches will also be essential to substantiate the signaling pathways responsible for the observed anticancer activity.

Future studies should further compare the efficacy of nano formulations with matched free-drug doses under physiologically relevant conditions, including serum-containing media and gastrointestinal or tumor-mimicking microenvironments, to better predict their translational potential.

Given the intrinsic colorimetric properties of curcumin and silibinin, compound-only controls and orthogonal cell viability assays should also be incorporated to eliminate potential optical interference and ensure that the observed biological effects accurately reflect changes in cellular viability.

In conclusion, the co-delivery of curcumin and silibinin via hyaluronic acid-functionalized PEGylated niosomes represents a promising nanotherapeutic strategy for colorectal cancer. By combining improved drug delivery with enhanced anticancer efficacy, this platform provides a strong foundation for future preclinical investigations and may contribute to the development of more effective targeted therapies for colorectal cancer.Overall, the co-delivery of curcumin and silibinin using hyaluronic acid-modified PEGylated niosomes represents a promising technique for CRC therapy

Ethical Approval

Experiments were approved by the Ethics Committee of the Hamadan University of medical sciences (1402/3/6-1953).

Acknowledgments

The authors would like to thank the Faculty of Medicine at Tabriz University of Medical Sciences for its technical support.

Conflict of interest

The authors declare that they have no conflict of interest.

funding

The authors declare that no funds were received during the preparation of this manuscript.

References:

1. Siegel RL, Wagle NS, Cercek A, Smith RA, Jemal A. Colorectal cancer statistics, 2023. *CA Cancer J Clin* 2023;73(3):233-54. doi: 10.3322/caac.21772
2. Morgan E, Arnold M, Gini A, Lorenzoni V, Cabasag CJ, Laversanne M, et al. Global burden of colorectal cancer in 2020 and 2040: incidence and mortality estimates from GLOBOCAN. *Gut* 2023;72(2):338-44. doi: 10.1136/gutjnl-2022-327736
3. Ejaz A, Pawlik TM. Contemporary Management of Metastatic Colorectal Cancer: A Precision Medicine Approach: Elsevier; 2025.
4. Anania G, Resta G, Marino S, Fabbri N, Scagliarini L, Marchitelli I, et al. Treatment of Colorectal Cancer: a Multidisciplinary Approach. *J Gastrointest Cancer* 2019;50(3):458-68. doi: 10.1007/s12029-018-0100-9

5. Leowattana W, Leowattana P, Leowattana T. Systemic treatment for metastatic colorectal cancer. *World J Gastroenterol* 2023;29(10):1569-88. doi: 10.3748/wjg.v29.i10.1569

6. Deshmukh R, Prajapati M, Harwansh RK. Management of Colorectal Cancer Using Nanocarriers-based Drug Delivery for Herbal Bioactives: Current and Emerging Approaches. *Curr Pharm Biotechnol* 2024;25(5):599-622. doi: 10.2174/0113892010242028231002075512

7. Mahmoudi A, Jamialahmadi T, Kesharwani P, Sahebkar A. Bioinformatic analysis of the molecular targets of curcumin in colorectal cancer. *Pathol Res Pract* 2024;262:155533. doi: 10.1016/j.prp.2024.155533

8. Liu W, Yang B, Yang L, Kaur J, Jessop C, Fadhil R, et al. Therapeutic effects of ten commonly used Chinese herbs and their bioactive compounds on cancers. *Evidence-Based Complementary and Alternative Medicine* 2019;2019(1):6057837.

9. Iranpoor N, Jafari-Gharabaghlou D, Abdulzehra S, Dashti MR, Gorbanzadeh F, Zarghami N. Development and Characterization of Curcumin Loaded PEGylated Niosomal Nanoparticles: Potential Anti-Cancer Effect on Breast Cancer Cells through RFC Gene Expression. *Asian Pac J Cancer Prev* 2025;26(3):1017-26. doi: 10.31557/APJCP.2025.26.3.1017

10. Nobari S, Najafi R, Mahdavinezhad A, Jalali A, Amini R. The Combination of Zerumbone with 5-Fluorouracil for Sensitizing Colorectal Cancer-Associated Fibroblasts to Treatment. *Evid Based Complement Alternat Med* 2022;2022:9369328. doi: 10.1155/2022/9369328

11. Zoi V, Galani V, Lianos GD, Voulgaris S, Kyritsis AP, Alexiou GA. The Role of Curcumin in Cancer Treatment. *Biomedicines* 2021;9(9):1086. doi: 10.3390/biomedicines9091086

12. Bhatia M, Bhalerao M, Cruz-Martins N, Kumar D. Curcumin and cancer biology: Focusing regulatory effects in different signalling pathways. *Phytother Res* 2021;35(9):4913-29. doi: 10.1002/ptr.7121

13. Ray PP, Islam MA, Islam MS, Han A, Geng P, Aziz MA, et al. A comprehensive evaluation of the therapeutic potential of silibinin: a ray of hope in cancer treatment. *Front Pharmacol* 2024;15:1349745. doi: 10.3389/fphar.2024.1349745

14. Roca E, Colloca G, Lombardo F, Bellieni A, Cucinella A, Madonia G, et al. The importance of integrated therapies on cancer: Silibinin, an old and new molecule. *Oncotarget* 2024;15:345-53. doi: 10.18632/oncotarget.28587

15. Jadid MFS, Jafari-Gharabaghlou D, Bahrami MK, Bonabi E, Zarghami N. Enhanced anti-cancer effect of curcumin loaded-niosomal nanoparticles in combination with heat-killed Saccharomyces cerevisiae against human colon cancer cells. *Journal of Drug Delivery Science and Technology* 2023;80:104167. doi: 10.1016/j.jddst.2023.104167

16. Singh CK, George J, Ahmad N. Resveratrol-based combinatorial strategies for cancer management. *Ann N Y Acad Sci* 2013;1290(1):113-21. doi: 10.1111/nyas.12160

17. Amirsaadat S, Jafari-Gharabaghlou D, Alijani S, Mousazadeh H, Dadashpour M, Zarghami N. Metformin and Silibinin co-loaded PLGA-PEG nanoparticles for effective combination therapy against human breast cancer cells. *Journal of Drug Delivery Science and Technology* 2021;61:102107. doi: 10.1016/j.jddst.2020.102107

18. Montgomery A, Adeyeni T, San K, Heuertz RM, Ezekiel UR. Curcumin Sensitizes Silymarin to Exert Synergistic Anticancer Activity in Colon Cancer Cells. *J Cancer* 2016;7(10):1250-7. doi: 10.7150/jca.15690

19. Dalimi-Asl S, Babaahmadi-Rezaei H, Mohammadzadeh G. Combination of Silibinin and Curcumin Reduced Leptin Receptor Expression in MCF-7 Human Breast Cancer Cell Line. *Iran J Med Sci* 2020;45(6):477-84. doi: 10.30476/ijms.2019.81934

20. Mahato M, Patra S, Gogoi M. Herbal Nanocarriers for cancer therapy. *Nanopharmaceuticals: Principles and Applications Vol 2* 2021:41-75.
21. Hani U, Gowda BJ, Siddiqua A, Wahab S, Begum MY, Sathishbabu P, et al. Herbal approach for treatment of cancer using curcumin as an anticancer agent: A review on novel drug delivery systems. *Journal of Molecular Liquids* 2023;390:123037.
22. Hazira RMN, Reddy MS. Niosomes: A nanocarrier drug delivery system. *GSC Biological and Pharmaceutical Sciences* 2023;22(2):120-7.
23. Liga S, Paul C, Moacă E-A, Péter F. Niosomes: Composition, Formulation Techniques, and Recent Progress as Delivery Systems in Cancer Therapy. *Pharmaceutics* 2024;16(2):223. doi: 10.3390/pharmaceutics16020223
24. Mehta S. Anti-cancer drugs targeting using nanocarrier niosomes-a review. *TMR Cancer* 2020;3(4):169-74.
25. Fu CP, Cai XY, Chen SL, Yu HW, Fang Y, Feng XC, et al. Hyaluronic Acid-Based Nanocarriers for Anticancer Drug Delivery. *Polymers (Basel)* 2023;15(10):2317. doi: 10.3390/polym15102317
26. Bashkeran T, Kamaruddin AH, Ngo TX, Suda K, Umakoshi H, Watanabe N, et al. Niosomes in cancer treatment: A focus on curcumin encapsulation. *Heliyon* 2023;9(8):e18710. doi: 10.1016/j.heliyon.2023.e18710
27. Phatak N, Bhattacharya S, Shah D, Manthalkar L, Sreelaya P, Jain A. CD44 targeted delivery of hyaluronic acid-coated polymeric nanoparticles against colorectal cancer. *Nanomedicine (Lond)* 2023;18(23):1613-34. doi: 10.2217/nnm-2023-0145
28. Jain S, Bharti S, Bhullar GK, Tripathi S. pH dependent drug release from drug conjugated PEGylated CdSe/ZnS nanoparticles. *Materials Chemistry and Physics* 2020;240:122162.
29. Ashrafizadeh M, Ahmadi Z, Mohammadinejad R, Farkhondeh T, Samarghandian S. Nano-soldiers Ameliorate Silibinin Delivery: A Review Study. *Curr Drug Deliv* 2020;17(1):15-22. doi:10.2174/1567201816666191112113031
30. Wang W, Li M, Wang L, Chen L, Goh BC. Curcumin in cancer therapy: Exploring molecular mechanisms and overcoming clinical challenges. *Cancer Lett* 2023;570:216332. doi: 10.1016/j.canlet.2023.216332
31. Ghumman SA, Ijaz A, Noreen S, Aslam A, Kausar R, Irfan A, et al. Formulation and Characterization of Curcumin Niosomes: Antioxidant and Cytotoxicity Studies. *Pharmaceuticals (Basel)* 2023;16(10):1406. doi: 10.3390/ph16101406
32. Alali U, Mohammed Kadhim Al-Tu'ma M, Fadhil Jawad A, Talib Ahmed S, Addai Ali H, Abdulzehra S, et al. Synthesis, Characterization, and In-Vitro Evaluation of Silibinin-loaded PEGylated Niosomal Nanoparticles: Potential Anti-Cancer Effects on SW480 Colon Cancer Cells. *Asian Pac J Cancer Prev* 2024;25(7):2539-50. doi: 10.31557/APJCP.2024.25.7.2539
33. Zhao Q, Bai J, Chen Y, Liu X, Zhao S, Ling G, et al. An optimized herbal combination for the treatment of liver fibrosis: Hub genes, bioactive ingredients, and molecular mechanisms. *J Ethnopharmacol* 2022;297:115567. doi: 10.1016/j.jep.2022.115567
34. Hannen R, Bartsch JW. Essential roles of telomerase reverse transcriptase hTERT in cancer stemness and metastasis. *FEBS Lett* 2018;592(12):2023-31. doi: 10.1002/1873-3468.13084
35. Pisani C, Ramella M, Boldorini R, Loi G, Billia M, Boccafoschi F, et al. Apoptotic and predictive factors by Bax, Caspases 3/9, Bcl-2, p53 and Ki-67 in prostate cancer after 12 Gy single-dose. *Sci Rep* 2020;10(1):7050. doi: 10.1038/s41598-020-64062-9
36. Nasiri M, Zarghami N, Koshki KN, Mollazadeh M, Moghaddam MP, Yamchi MR, et al. Curcumin and silibinin inhibit telomerase expression in T47D human breast cancer cells. *Asian Pac J Cancer Prev* 2013;14(6):3449-53. doi: 10.7314/apjcp.2013.14.6.3449

37. Brentnall M, Rodriguez-Menocal L, De Guevara RL, Cepero E, Boise LH. Caspase-9, caspase-3 and caspase-7 have distinct roles during intrinsic apoptosis. *BMC cell biology* 2013;14:1-9.
38. Chen H, Yang X, Feng Z, Tang R, Ren F, Wei K, et al. Prognostic value of Caspase-3 expression in cancers of digestive tract: a meta-analysis and systematic review. *Int J Clin Exp Med* 2015;8(7):10225-34.
39. Jun SY, Kim J, Yoon N, Maeng LS, Byun JH. Prognostic Potential of Cyclin D1 Expression in Colorectal Cancer. *J Clin Med* 2023;12(2):572. doi: 10.3390/jcm12020572
40. Amirsaadat S, Jafari-Gharabaghlou D, Dadashpour M, Zarghami N. Potential anti-proliferative effect of nano-formulated curcumin through modulating micro RNA-132, Cyclin D1, and hTERT genes expression in breast cancer cell lines. *Journal of Cluster Science* 2023;34(5):2537-46. doi: 10.1007/s10876-023-02404-z
41. Binienda A, Ziolkowska S, Pluciennik E. The Anticancer Properties of Silibinin: Its Molecular Mechanism and Therapeutic Effect in Breast Cancer. *Anticancer Agents Med Chem* 2020;20(15):1787-96. doi: 10.2174/1871520620666191220142741
42. Neophytou CM, Trougakos IP, Erin N, Papageorgis P. Apoptosis Deregulation and the Development of Cancer Multi-Drug Resistance. *Cancers (Basel)* 2021;13(17):4363. doi: 10.3390/cancers13174363
43. Yu C, Yang B, Najafi M. Targeting of cancer cell death mechanisms by curcumin: Implications to cancer therapy. *Basic Clin Pharmacol Toxicol* 2021;129(6):397-415. doi: 10.1111/bcpt.13648
44. Sameri S, Mohammadi C, Mehrabani M, Najafi R. Targeting the hallmarks of cancer: the effects of silibinin on proliferation, cell death, angiogenesis, and migration in colorectal cancer. *BMC Complement Med Ther* 2021;21(1):160. doi: 10.1186/s12906-021-03330-1
45. Mollazadeh S, Al-Asady AM, Barjasteh A, Latifi H, Avan A, Khazaei M, et al. Niosomes as a Promising Therapeutic Approach against Colorectal Cancer: A Focus on the Delivery of Chemotherapeutics and Natural Products. *Current Pharmaceutical Design* 2024;30(21):1659-66. doi: 10.2174/0113816128303645240429052835.PMID
46. Akram A, Sakhawat A, Ghani MU, Khan MU, Rehman R, Ali Q, et al. Silibinins and curcumin as promising ligands against mutant cystic fibrosis transmembrane regulator protein. *AMB Express* 2024;14(1):84.
47. Barros TMB, Lima APB, Almeida TC, da Silva GN. Inhibition of urinary bladder cancer cell proliferation by silibinin. *Environ Mol Mutagen* 2020;61(4):445-55. doi: 10.1002/em.22363
48. Chavda VP, Nalla LV, Balar P, Bezbaruah R, Apostolopoulos V, Singla RK, et al. Advanced Phytochemical-Based Nanocarrier Systems for the Treatment of Breast Cancer. *Cancers (Basel)* 2023;15(4):1023. doi: 10.3390/cancers15041023
49. Jahanafrooz Z, Motamed N, Rinner B, Mokhtarzadeh A, Baradaran B. Silibinin to improve cancer therapeutic, as an apoptotic inducer, autophagy modulator, cell cycle inhibitor, and microRNAs regulator. *Life sciences* 2018;213:236-47.
50. Pricci M, Girardi B, Giorgio F, Losurdo G, Ierardi E, Di Leo A. Curcumin and Colorectal Cancer: From Basic to Clinical Evidences. *Int J Mol Sci* 2020;21(7):2364. doi: 10.3390/ijms21072364